Journal of Geoscience and Environment Protection, 2026, 14(2), 76-90
https://www.scirp.org/journal/gep
ISSN Online: 2327-4344
ISSN Print: 2327-4336

Analysis of the Monthly-Scale Air-Sea Causes for the 2020 Summer Rainfall over the Middle-Lower Yangtze River

Wanting Yu, Wei Wang*

Climate Change and Resource Utilization in Complex Terrain Regions Key Laboratory of Sichuan Province, School of Atmospheric Sciences, Chengdu University of Information Technology, Chengdu, China
Email: *985736089@qq.com

How to cite this paper: Yu, W. T., & Wang, W. (2026). Analysis of the Monthly-Scale Air-Sea Causes for the 2020 Summer Rainfall over the Middle-Lower Yangtze River. *Journal of Geoscience and Environment Protection, 14,* 76-90.
https://doi.org/10.4236/gep.2026.142005

Received: February 14, 2026
Accepted: February 2, 2026
Published: February 5, 2026

Abstract

From a month-to-month evolution perspective, this study analyzes changes in atmospheric circulation and the forcing effects of three-dimensional thermal structures such as oceanic heat content during the summer of 2020, using ERA5, OISST, and SODA reanalysis datasets. The results show that in June, the double warm-core structure of the warm pool drove adjustments in atmospheric circulation and moisture transport, leading to anomalously high Meiyu rainfall in the area north of the Yangtze River. In July, as the thermal forcing of the warm pool peaked, the atmospheric circulation further intensified and generated strong low-level wind convergence, resulting in a precipitation increase of approximately 90% in the middle and lower reaches of the basin. Entering August, the thermal structure of the western Pacific warm pool underwent reorganization. The weakening of its heat source induced an eastward retreat of the subtropical high and a decay in moisture transport, ultimately causing reduced precipitation over the middle and lower reaches of the Yangtze River. In summary, this study reveals the key "three-dimensional oceanic thermal forcing–atmospheric circulation response–regional precipitation" mechanism responsible for precipitation anomalies in the region. This provides a novel and diagnostic perspective for a deeper understanding of extreme precipitation events under Western Pacific Warm Pool thermal conditions.

Keywords

Middle and Lower Reaches of the Yangtze River, Precipitation, Western Pacific Warm Pool, Western Pacific Subtropical High, South Asian High

1. Introduction

The Yangtze River Basin is one of the most densely populated and economically developed regions in China. Located in the mid- to low-latitude subtropical zone, it represents a typical monsoon climate region in eastern China (Bai et al., 2025; Zhao & Zhou, 2024). In recent decades, the basin has experienced more frequent extreme weather and climate events, posing serious challenges to regional socio-economic development and ecological security (Li et al., 2021). From June to August each year, the intensity, duration, and spatial distribution of precipitation directly determine the regional drought-flood patterns. Meiyu is closely linked to the synergistic effects of key factors such as the evolution of the Western Pacific Subtropical High (WPSH), adjustments in mid-latitude circulation, and anomalies in moisture transport (Ding et al., 2007) Under global warming, extreme events triggered by rainfall have become more frequent and intense (Jiang et al., 2022). Therefore, elucidating the causes of extreme precipitation in the Yangtze River Basin is of critical importance for understanding regional climate anomaly mechanisms and enhancing disaster prevention and mitigation capabilities.

In recent years, extreme weather events have frequently occurred during the summer in the Yangtze River basin. The summer of 2020 represents a particularly typical case, characterized by an exceptionally severe "Violent Meiyu" episode. The Meiyu season persisted for 52 days, delivering an average precipitation of 753.9 mm, which is approximately 1.5 times the climatological mean (Liu & Ding, 2020; Wang et al., 2020). This resulted in severe flooding and significant economic losses, making it a key case for studying extreme Meiyu processes. Scholars have investigated this extreme event from various perspectives, with some focusing on monthly or seasonal mean signals. Liu et al. (2021) analyzed June-July and August 2020 as separate periods and pointed out that the phase transition of atmospheric intraseasonal oscillation led to the shift of the main rain belt from a north-south to a southwest-northeast orientation. By focusing on the influence of sea surface temperature (SST), Zheng and Wang (2021) indicated that prior SST anomalies in the northwestern Atlantic had predictive significance for precipitation in the Yangtze River Basin in June. Another category of research focuses on characterizing the evolution of processes at the daily timescale. Ma et al. (2022), through daily analysis, divided June-July into two distinct stages, revealing the relationship between rain belt evolution and synoptic-scale atmospheric circulation adjustments. Tang et al. (2022) examined the average distribution characteristics of precipitation across the basin from a spatial zoning perspective.

While existing studies have deepened the understanding of the extreme Meiyu event in 2020, most analyses have focused on specific periods such as June-July, seasonal averages, or daily-scale processes. Such approaches are often unable to fully reveal the dynamic processes linking SST anomalies and precipitation at the monthly scale. Therefore, this study adopts a monthly-scale perspective. It compares precipitation, circulation, and moisture conditions across the summer months and links these atmospheric changes to the month-to-month evolution of

the three-dimensional oceanic thermal structure (e.g., warm water volume and heat content). Through this integrated analysis, we systematically elucidate how oceanic thermal forcing drives atmospheric circulation adjustments and ultimately regulates the evolution of extreme precipitation anomalies over the Yangtze River Basin in 2020.

The remainder of this paper is structured as follows. Section 2 describes the datasets and methodology used. Section 3 examines the monthly characteristics of precipitation and temperature anomalies from June to August 2020. Section 4 investigates the causes of the monthly atmospheric circulation anomalies. Section 5 analyzes the evolution of sea surface temperature and three-dimensional oceanic thermal structure, along with the monthly variations in vertical circulation. Finally, Section 6 presents the main conclusions and provides a discussion.

2. Data and Methods

2.1. Data

Precipitation and atmospheric circulation data are sourced from the ERA5 reanalysis dataset provided by the European Centre for Medium-Range Weather Forecasts (ECMWF), with a spatial resolution of 0.25˚ × 0.25˚ (Hersbach et al., 2020). Sea surface temperature data are obtained from the daily Optimum Interpolation Sea Surface Temperature (OISST) version 2.1 reanalysis product provided by the National Oceanic and Atmospheric Administration (NOAA) (Huang et al., 2020). The three-dimensional oceanic thermal structure data are derived from the monthly Simple Ocean Data Assimilation (SODA) dataset (version 3.15.2), jointly developed by the University of Maryland and Texas A&M University (Carton & Giese, 2008). The monthly Niño 3.4 index for 2020 was obtained from the National Oceanic and Atmospheric Administration Climate Prediction Center (NOAA CPC) (https://www.cpc.ncep.noaa.gov/products/CDB/CDB_Archive_html/bulletin_112020/Tropics/table2.shtml).

2.2. Methods

The vertically integrated atmospheric water vapor flux vector Q is calculated as:

$$F = -\frac{1}{g}\int_{P_S}^{P_t} \overline{V} q \mathrm{d}p \tag{1}$$

where $\overline{V}$ is the horizontal wind vector, q is the specific humidity, P_S and P_t are respectively the pressure at the bottom boundary (surface pressure) and the top boundary (set to 1 hPa) of the atmospheric column. The unit of F is kg (m·s)$^{-1}$.

Following the methodology of Huang et al. (2021), this study employs the meridional mass streamfunction to characterize the atmospheric circulation over the Yangtze River Basin:

$$\psi = \frac{2\pi R \cos\phi}{g}\int_0^p [V_d]\mathrm{d}p \tag{2}$$

where, $[V_d]$ represents the zonal-mean meridional divergent wind over a speci-

fied region; ψ, R, ϕ, g, and p denote the meridional mass streamfunction, the Earth's radius, the latitude, the acceleration of gravity, and the barometric pressure, respectively.

In addition, the meridional second order gradient of sea surface temperature anomalies, $-\frac{\partial^2(\Delta SST)}{\partial y^2}$ is used to quantify the variability and spatial distribution characteristics of its meridional structure.

The Yangtze River Basin domain in this study is defined as 28˚N-34˚N, 105˚E-122.5˚E. The Western Pacific Warm Pool (WPWP) is defined as the region within 30˚S-30˚N and 120˚E-180˚E where the sea surface temperature exceeds 28˚C. The analysis period covers the summer months (June-August) of 2020, and the climatological mean is based on the 42-year average from 1982 to 2023.

3. Comparison of Precipitation Characteristics

Figure 1 shows the spatial distributions of the monthly precipitation and temperature anomaly percentages for June-August 2020. Precipitation over the middle and lower reaches of the Yangtze River is generally characterized by above-normal conditions early and below-normal conditions later in the summer. In June, the rain belt is located farther north than usual, resulting in above-normal precipitation

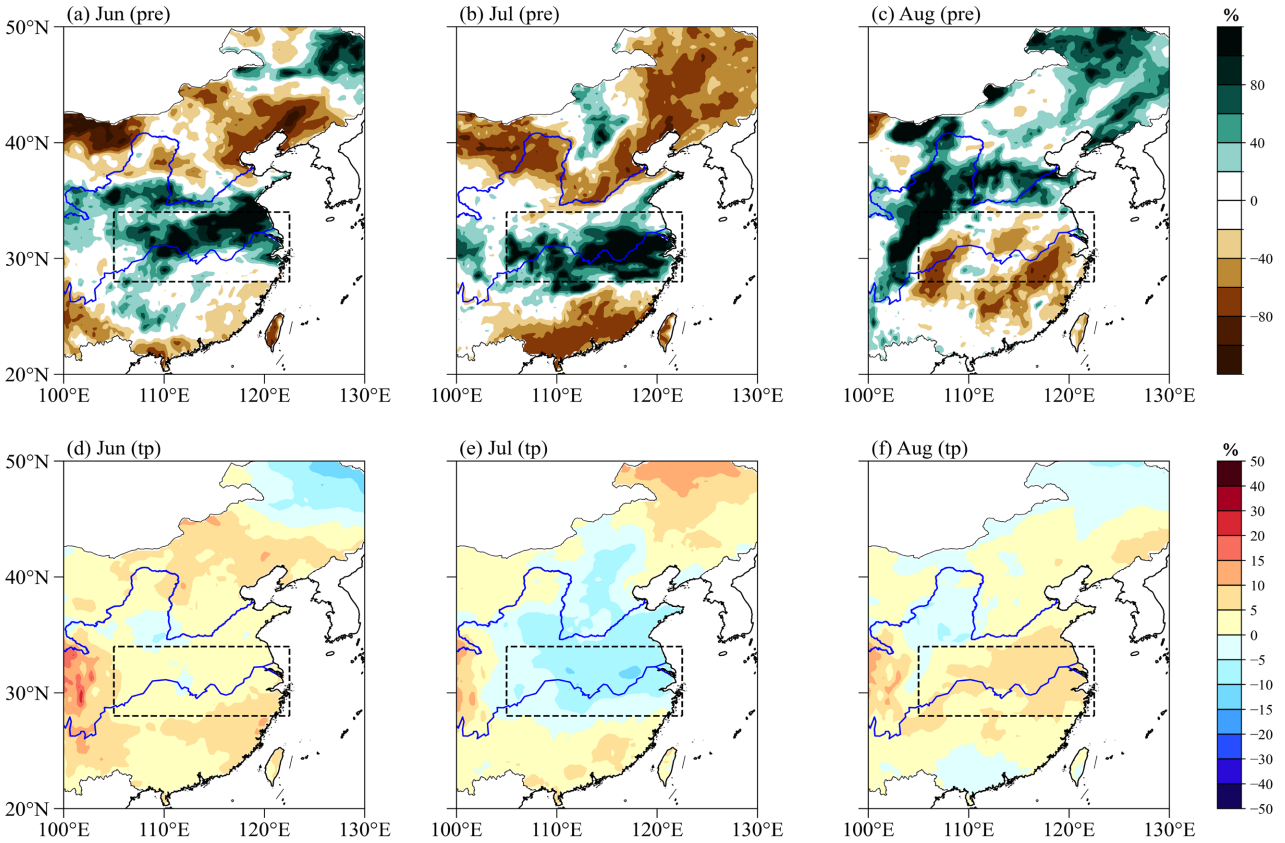

Figure 1. Monthly (a)-(c) precipitation and (d)-(f) temperature anomaly percentages (units: %) from June to August 2020. The black rectangle denotes the study domain of 28˚-34˚N, 105˚-122.5˚E.

and temperatures about 5% higher north of the Yangtze River (**Figure 1(a)**, **Figure 1(d)**). In July, the rain belt remains quasi-stationary over the middle and lower reaches of the basin. Precipitation exceeds the climatological mean by 90%, marking the seasonal peak, while temperatures were approximately 10% lower (**Figure 1(b)**, **Figure 1(e)**). By August, the Meiyu season has ended, leading to a southward concentration of precipitation south of the Yangtze River with deficits of 20% - 40% and a rise in temperatures (**Figure 1(c)**, **Figure 1(f)**). Overall, the region exhibits a "high temperature and high humidity" pattern during the August.

4. Analysis of the Causes of Atmospheric Circulation Anomalies

During the summer of 2020, both the South Asian High (SAH) and the WPSH exhibited persistently stronger-than-normal intensities and more eastward positions. These two systems interact with a mid-to-high latitude blocking pattern, collectively providing a stable circulation background for precipitation in the Yangtze River Basin (Gong & He, 2006). In June, the SAH extends eastward in a zonal-oriented pattern, dominating the middle and upper reaches of the Yangtze River. Meanwhile, the WPSH extends westward, with its northern boundary located farther north than the climatological mean (**Figure 2(a)**, **Figure 2(d)**). During this period, the mid-to-high latitudes exhibit a "two ridges and two troughs" pattern. The Ural Mountain ridge guides cold air southward, which converges with the warm and moist airflow on the northwestern flank of the WPSH over the middle and lower reaches of the Yangtze River. This convergence

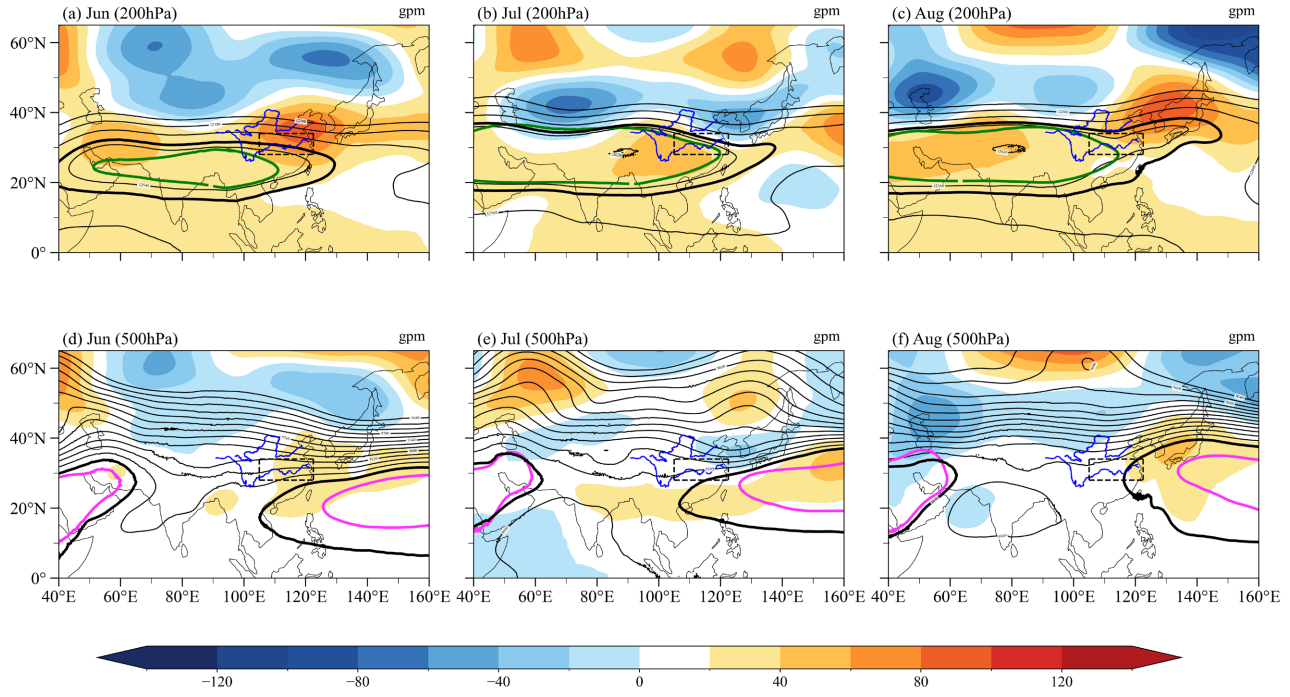

Figure 2. Monthly (a)-(c) 200-hPa and (d)-(f) 500-hPa geopotential height (contours; units: gpm) and their anomalies (shading) from June to August 2020. The green and pink contours denote the climatological 12520 gpm and 5880 gpm lines, respectively.

provides favorable dynamic conditions for heavy rainfall in this region.

Under further adjustment of the circulation systems, the SAH continues to extend eastward and steadily covers the middle and lower reaches of the Yangtze River. The WPSH maintains its westward extension, with its westernmost ridge point reaching the farthest westward position of the summer, placing the middle and lower reaches of the Yangtze River at the northwestern edge of the high (**Figure 2(b)**, **Figure 2(e)**). Meanwhile, the Okhotsk Sea blocking high strengthens significantly, leading to increased activity of cold air. This cold air interacts with the convergent ascent along the western edge of the WPSH, resulting in persistently above-normal precipitation over the middle and lower reaches of the Yangtze River. In August, the SAH exhibits a pronounced eastward and northward shift, while the WPSH weakens and retreats eastward in a more fragmented, block-like structure (**Figure 2(c)**, **Figure 2(f)**). Concurrently, the meridional flow in the mid-to-high latitudes weakens, and the circulation transitions to a "two-trough-one-ridge" pattern. This reduces the convergence between cold and warm air masses, leading to a rapid decay of dynamic support for precipitation over the Yangtze River Basin and a consequent decline in rainfall.

Anomalies in the low-level wind field and the associated modulated water vapor transport exhibit distinct monthly evolution patterns, which directly regulate the sub-seasonal differences in precipitation over the Yangtze River Basin. In June, the South China Sea and the northwestern Pacific are dominated by an anomalous anticyclone (**Figure 3(a)**, **Figure 3(d)**). The intensified southwesterly

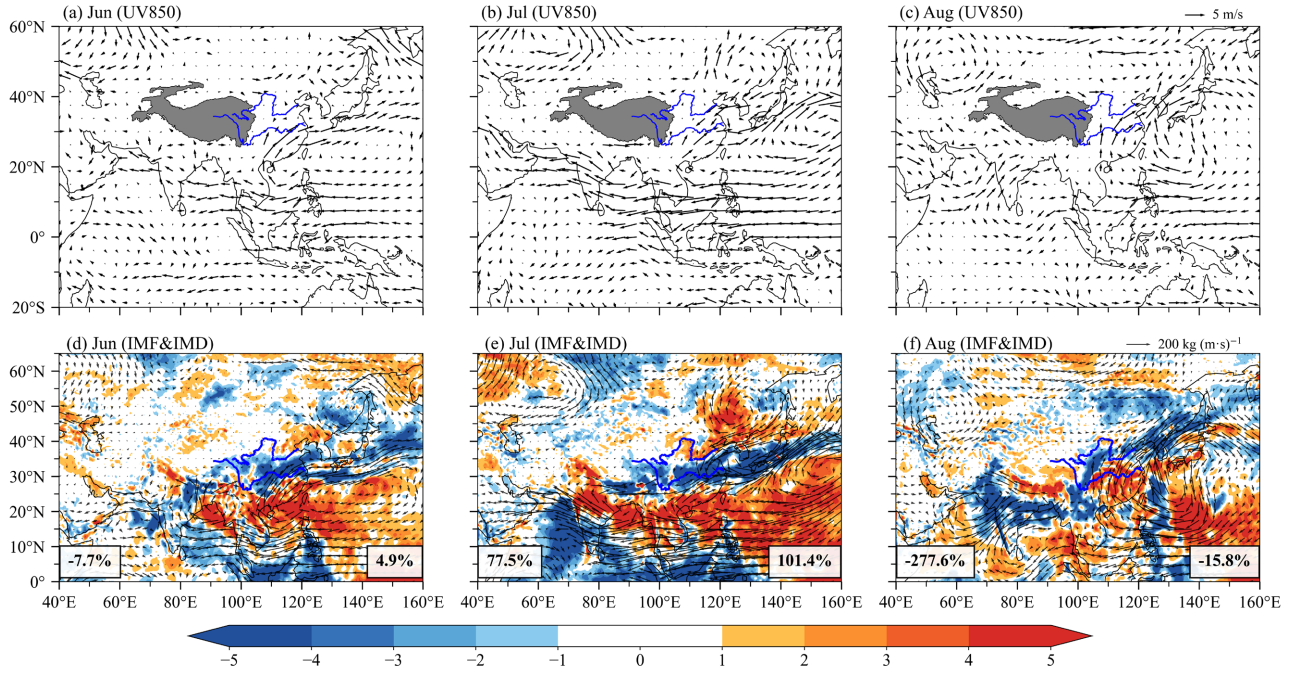

Figure 3. Monthly (a)-(c) 850-hPa horizontal wind anomalies (vectors; units: $m \cdot s^{-1}$) and (d)-(f) vertically integrated (surface to 300 hPa) moisture flux anomalies (vectors; units: $kg \cdot m^{-1} \cdot s^{-1}$) along with moisture flux divergence anomalies (shading; units: 10^{-5} $kg \cdot m^{-2} \cdot s^{-1}$) from June to August 2020 and 2022. The numbers in the panels indicate the percentage anomalies of the total moisture flux along the 80˚E and 140˚E meridians (averaged over 20˚-30˚N).

jet on its western flank interacts with moisture supplied from the western Pacific, transporting abundant moisture to the middle and lower reaches of the Yangtze River. A distinct zonal-oriented convergent zone in moisture flux divergence develops over the region, providing ample moisture conditions for heavy precipitation.

In July, the southwesterly winds on the western flank of the anomalous anticyclone over the northwestern Pacific and the northeasterly winds on the western side of the Yellow Sea cyclone converge, leading to a significant enhancement of vertical upward motion (**Figure 3(b)**, **Figure 3(e)**). Moisture transport intensity reaches its peak, with contributions from the Bay of Bengal and the western Pacific increasing approximately 77.5% and 101.4% above climatological levels, respectively. The convergence of moisture flux expands in coverage and intensifies in magnitude, directly sustaining the persistent heavy rainfall during the Meiyu period in this region. In August, although the anomalous anticyclone over the northwestern Pacific persists, the southerly jet on its western flank weakens markedly, resulting in inadequate dynamic forcing for moisture transport (**Figure 3(c)**, **Figure 3(f)**). Consequently, the vertically integrated moisture flux turns divergent, which suppresses precipitation and leads to a subsequent decline in rainfall over the middle and lower reaches of the Yangtze River.

5. Sea Surface Temperature Anomaly Forcing

Tropical SST anomalies are a key driver of summer climate variability in the Western Pacific-East Asia region (Wang et al., 2000; Ou et al., 2022). The previous section revealed the monthly variations in circulation and precipitation during the summer of 2020. This subsection focuses on key oceanic drivers, emphasizing the three-dimensional thermal structure of the ocean (e.g., warm-water volume and heat content). By integrating sea surface temperature and regional Hadley circulation in a comparative analysis, we explore how sea surface temperature anomalies ultimately regulate the monthly evolution of precipitation in the Yangtze River Basin through their influence on atmospheric circulation.

5.1. Evolution of Sea Surface Temperature

2020 is a typical year of transition from El Niño to La Niña (Cao et al., 2022). The Niño3.4 index fell from +0.5˚C to −0.2˚C between April and May, indicating the rapid decay of El Niño. Subsequently, La Niña conditions developed and persisted through the summer (June-August), with the index remaining consistently negative. In the year following an El Niño event, the East Asian summer monsoon tends to be weaker, which favors above-normal precipitation over the Yangtze River Basin (Wang et al., 2020). Following the onset of La Niña in spring, an "east cool, west warm" SST pattern dominates its evolution throughout the summer (**Figure 4**). In June, a strong but spatially confined cold anomaly emerges in the equatorial eastern Pacific, marking the establishment of a La Niña signal. By July, the cold core expands westward with reduced intensity, while warming in the

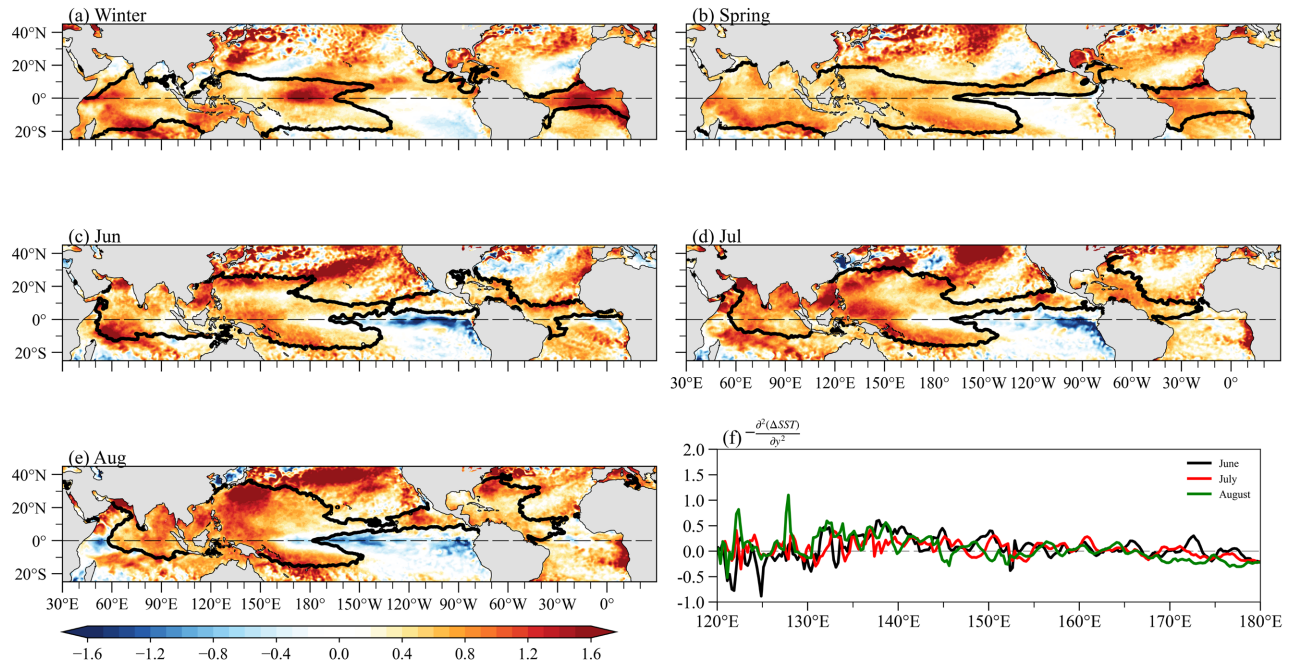

Figure 4. (a)-(e) Sea surface temperature anomalies (unit: ˚C) before and during summer (June–August) 2020, and (f) monthly variation of the meridional second-order derivative of SST anomalies averaged over 5˚S - 5˚N (unit: 10^{-11} ˚C·m^{-2}). The black line indicates the 28˚C isotherm.

WPWP and the Indian Ocean further intensifies. In August, the La Niña type cold SST expands westward to approximately 150˚E, and warm pool warming reaches its peak. Accompanying this evolution, the spatial extent of the 28˚C isotherm expands month by month, reaching its maximum in August, reflecting the continuous accumulation of heat within the warm pool.

The aforementioned "east cool, west warm" SST pattern, particularly the anomalous warming in the WPWP, provides important thermal forcing for circulation anomalies such as the westward extension and northward shift of the WPSH by exciting convective activity (Li et al., 2007). This thermal background is further corroborated by the month-to-month evolution of the meridional second order gradient of SST anomalies (**Figure 4(f)**): its variability within the key region of 120˚E-130˚E peaks in August, while the gradient east of 145˚E fluctuates slightly around zero and flattens most noticeably in August. This behavior is consistent with the weakened SST gradient in the eastern equatorial Pacific during the developing phase of La Niña.

The progressive expansion of the 28˚C isotherm in **Figure 4** visually reflects the continuous horizontal accumulation of warm water in the western Pacific during the summer of 2020. To more systematically characterize the evolution of the thermal structure of the WPWP, this study further analyzes the monthly variations in both the volume and three-dimensional spatial distribution of water warmer than 28˚C (used here as the criterion for defining the warm pool) (Wu et al., 2014).

In June, the core of the warm water is mainly located in the Northern Hemi-

sphere (Figure 5(a)). Two shallow high temperature centers with maximum values reaching 31.5˚C are present near 120˚E, 20˚N, representing the northernmost position of such warm cores during the summer. Meanwhile, a columnar region of high temperature warm water with a thickness of approximately 120 m is observed along the equator around 120˚E, reflecting the vertical thermal structure of the tropical warm pool. Around 30˚N, the warm water exhibits a zonal banded distribution, with temperatures decreasing eastward from 120˚E. The main body of the warm water is primarily concentrated in the coastal seas east of China.

In July, the meridional extent of the high temperature center near 120˚E, 20˚N expands noticeably, while the columnar warm water region along the equator persists (Figure 5(b)). The area of warm water deeper than 28˚C expands in the Northern Hemisphere, indicating a further concentration of warm water toward the Northern Hemisphere. Meanwhile, SSTs in the near surface layer (120˚-130˚E) continue to rise.

In August, warm water in the Northern Hemisphere exhibits the characteristics of deep layer northward expansion and lateral shifting. SSTs across the western Pacific generally increase, while the spatial extent and intensity of subsurface warm water strengthen markedly. A meridionally oriented warm water belt with considerable depth develops near 130˚E (Figure 5(c)).

Meanwhile, the volume of warm water in the Northern Hemisphere showed a partial recovery. However, owing to the contraction of warm water in the equatorial region and the Southern Hemisphere, the total warm water volume in August is slightly lower than that in June. This volumetric contraction trend likely reflects modulation by the La Niña event of that year (Chen et al., 2024). The northward and subsurface shift of the main warm water body during the summer months clearly delineates the phased evolution of the three-dimensional thermal structure of the WPWP. Furthermore, analysis based on the summer long-term series (1982-2023) shows that the area-mean sea surface temperature over the WPWP is significantly positively correlated with the precipitation index over the Yangtze River Basin (r = 0.29, significant at the 90% confidence level), providing statistical support for the intrinsic linkage between oceanic temperature variation and regional precipitation. The evolution of this three-dimensional thermal structure thus furnishes a critical thermal-forcing background for subsequently modulating regional atmospheric circulation.

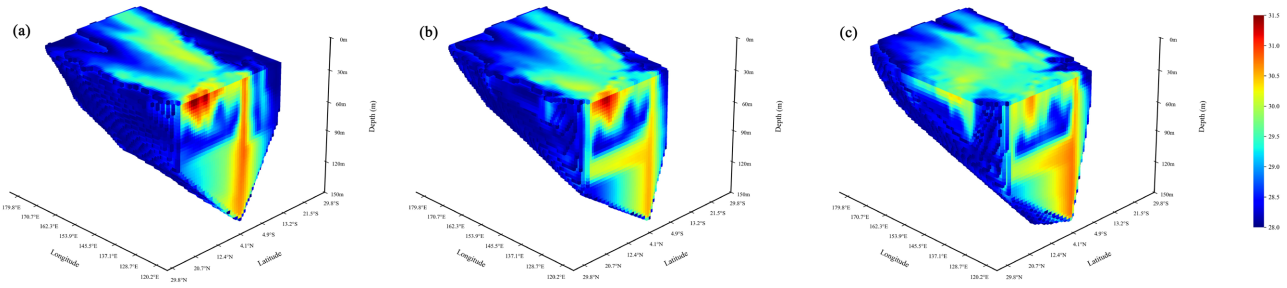

Figure 5. Evolution of the three-dimensional sea temperature (≥28˚C) in the western Pacific warm pool from June to August 2020.

5.2. Vertical Circulation Structure

Variations in warm-pool heat content can influence tropical and mid-to-high-latitude climate by modulating the Hadley circulation and the WPSH (Huang & Sun, 1994). Based on the monthly evolution of the three-dimensional oceanic thermal structure described above, this subsection first analyzes the month-to-month changes in the regional mass streamfunction over a broad domain (30˚S-30˚N).

To capture differences in circulation structures, we conducted monthly analyses from June to August for two adjacent Pacific regions: 123˚E -135˚E and 135˚E-145˚E. In June, the 123˚E-135˚E region featured an ascending branch near the equator and another near the subtropics (approximately 28˚N), with the latter being relatively weaker in intensity; the low latitudes of the Northern Hemisphere exhibit a pronounced positive double-center structure. In contrast, the circulation in the 135˚E-145˚E region is generally more dispersed, with multiple weaker ascending branches of limited vertical extent located in the low latitudes (**Figure 6(c)** & **Figure 6(d)**). In July, within the 123˚E-135˚E region, the morphology of the Northern Hemisphere Hadley cell remains similar to that in June, but its intensity notably strengthens, and the ascending branch shifts southward to approximately 25˚N. In the 135˚E-145˚E region, the circulation remains relatively

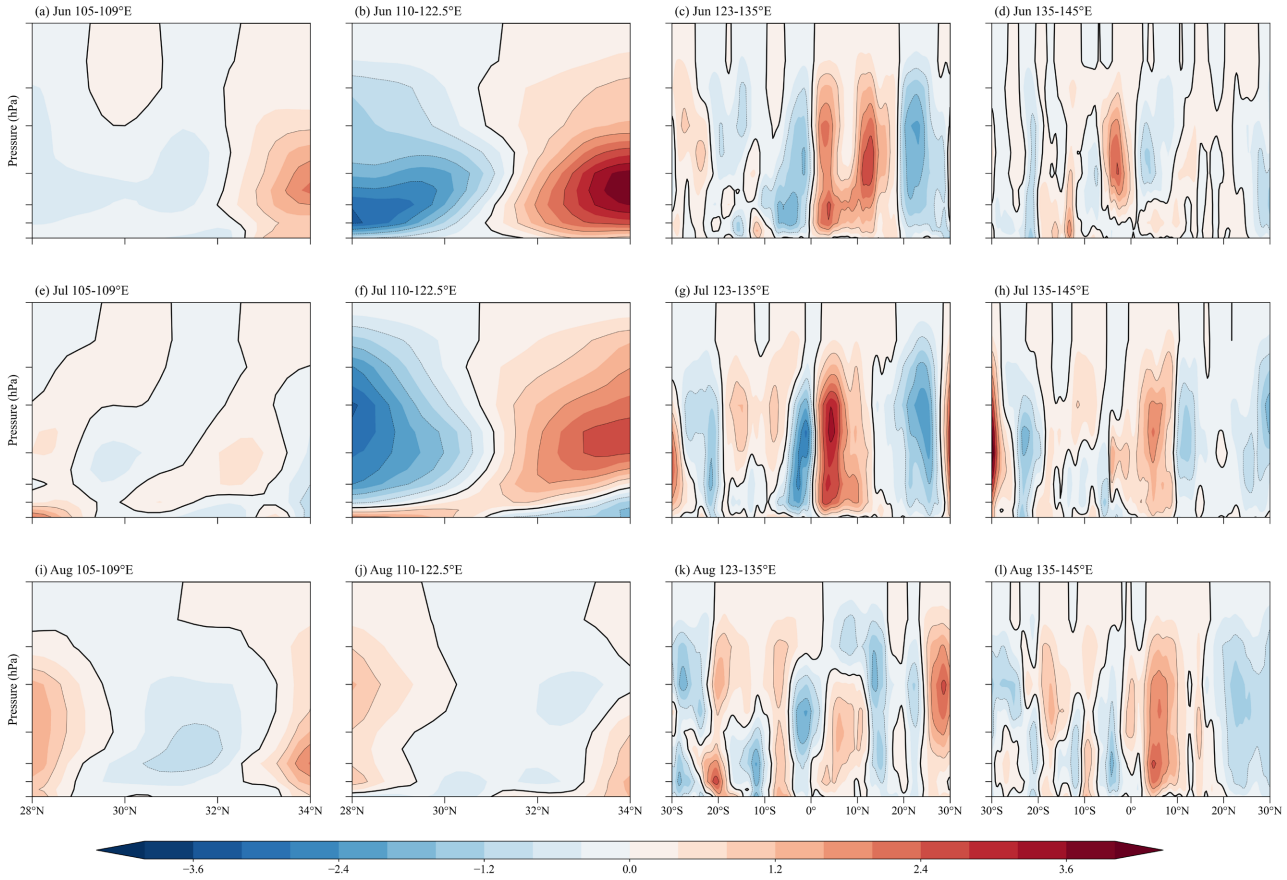

Figure 6. Regional mass streamfunction for June-August 2020, averaged over the longitude bands of (a), (e), (i) 105˚E-109˚E, (b), (f), (j) 110˚E-122.5˚E, (c), (g), (k) 123˚E-135˚E, and (d), (h), (l) 135˚E-145˚E, respectively.

dispersed, and the intensity of the ascending branches weakens further compared to June (Figure 6(g) & Figure 6(h)). In August, the circulation structure undergoes a distinct adjustment. In the 123˚E-135˚E region, the meridional structure of the Northern Hemisphere Hadley cell becomes more diffuse, with its ascending branch shifting southward to around 24˚N. Conversely, in the 135˚E-145˚E region, the area previously characterized by ascending motion transitions to domination by descending motion, while the ascending branch in the Northern Hemisphere weakens and is located near 12˚N (Figure 6(k) & Figure 6(l)).

To further investigate the direct influence of the Hadley circulation on precipitation over the Yangtze River Basin, the regional mass streamfunction is analyzed separately for its upper reaches (105˚E-109˚E) and its middle and lower reaches (110˚E-122.5˚E). The results show that its circulation structure also exhibits significant month-to-month differences. In June, the ascending branch of the Hadley cell over the upper reaches is located near 32˚N. Coupled with an upper-level anticyclone overlying a low-level cyclone around 29˚N, this structure provides favorable dynamic conditions for precipitation (Figure 6(a)). Over the middle and lower reaches, the circulation intensifies, with the ascending branch remaining stable near 31˚N, thereby offering additional support for rainfall (Figure 6(b)).

In July, the coherence of the circulation is enhanced. Over the upper reaches, the Hadley cell exhibits a dual ascending branch structure, with the region between 31˚N-32˚N showing a favorable configuration of upper-level divergence coupled with lower-level convergence. Meanwhile, the circulation over the middle and lower reaches continued to intensify, coordinating with the upstream circulation to jointly reinforce the regional ascending motion and precipitation conditions (Figure 6(e) & Figure 6(f)). In August, a shift in the circulation occurs. Over the upper reaches, the area near 30˚N transitions to weaker upper-level convergence and lower-level divergence, suppressing convective development. While an ascending branch persists near 32˚N, the overall dynamic structure becomes less favorable for precipitation. Concurrently, the region between 31˚N-34˚N over the middle and lower reaches is generally dominated by upper-level convergence and lower-level divergence, directly inhibiting ascending motion and leading to reduced rainfall in that month (Figure 6(i) & Figure 6(j)).

In summary, in June, the Hadley circulation over the 123˚E-135˚E oceanic region exhibits dual ascending branches near the equator and around 28˚N. This corresponds to a stable ascending branch and low-level convergence over the Yangtze River Basin, providing favorable circulation conditions for the first episode of heavy rainfall during the Meiyu season. In July, although the ascending branch weakens in the 135˚E-145˚E region, the Hadley circulation in the 123˚E-135˚E sector intensifies significantly with its ascending branch shifting southward to 25˚N. Concurrently, the circulation over the Yangtze River Basin strengthens overall with coordinated activity between its upper and lower reaches, jointly supporting the maintenance and enhancement of Meiyu rainfall. By August, the circulation structure over the oceanic regions becomes more diffuse, with the as-

cending branches shifting farther south. Consequently, the circulation over the Yangtze River Basin transitions to one dominated by subsidence or divergence. This shift in the circulation configuration collectively leads to a rapid decay of the dynamic conditions for precipitation.

6. Conclusions and Discussions

Adopting a monthly-scale perspective, this study elucidates the causes of the month-to-month precipitation anomalies over the Yangtze River Basin in the summer of 2020 by analyzing the forcing effect of the three-dimensional oceanic thermal structure and its induced three-dimensional atmospheric circulation response (Figure 7). The main conclusions are as follows:

1) Precipitation over the Yangtze River Basin during the summer of 2020 exhibits pronounced intraseasonal phase characteristics: During the Meiyu period from June to July, rainfall in the middle and lower reaches is persistently and anomalously high, with July precipitation exceeding the climatological mean by

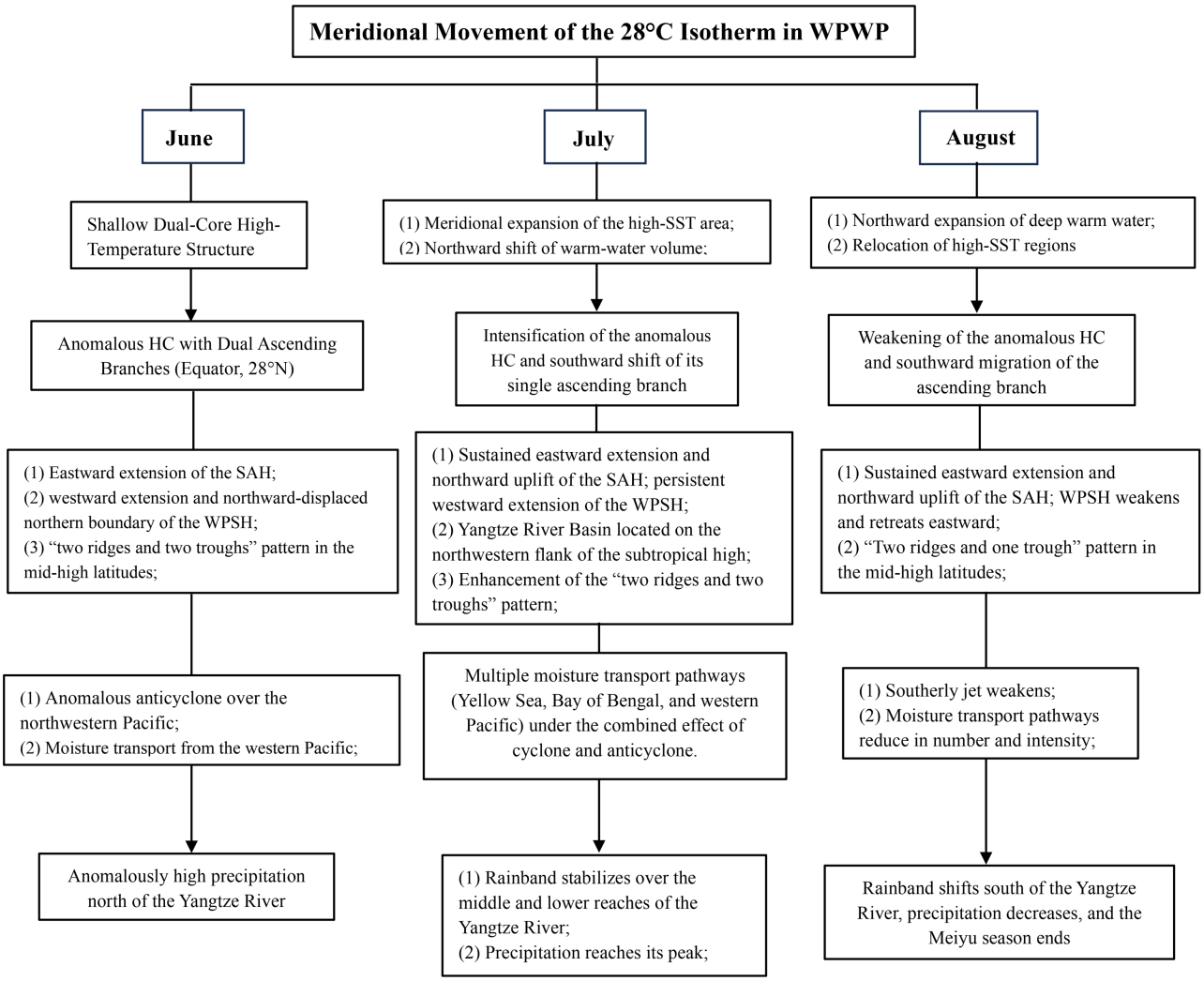

Figure 7. Schematic of the month-to-month precipitation evolution mechanism for June-August 2020.

approximately 90% and accompanied by below-normal temperatures. In August, following the end of the Meiyu season, precipitation decreases markedly, and temperatures rebounds accordingly.

2) In June, the warm pool in the Northern Hemisphere exhibits a shallow dual-core warm structure. The strong oceanic heat source released from this configuration drives the atmosphere, leading to an anomalous Hadley circulation with a dual ascending branch structure positioned anomalously northward. This thermally driven ascending motion and its associated upper-level divergence promote the eastward extension of the SAH and strengthen the WPSH. Simultaneously, an anomalous anticyclone establishes itself over the northwestern Pacific. The southwesterly flow on its western flank, together with moisture from the western Pacific, forms an intensive moisture transport belt. This results in anomalously high precipitation north of the Yangtze River, marking the onset of the Meiyu season.

3) In July, the thermal state of the warm pool intensifies further and becomes more concentrated with a northward expansion. The enhanced heat source drives a marked strengthening of the Hadley circulation, whose ascending branch shifts southward to around 25˚N. Both the SAH and the WPSH continue to intensify. Under the combined influence of the subtropical high's marginal control and the SAH's stable coverage, strong wind convergence between southwesterlies and northeasterlies occurs over the middle and lower reaches of the Yangtze River. Both moisture transport and vertical ascending motion peak, resulting in the highest precipitation of the summer in this region.

4) In August, the spatial extent and intensity of surface warm water reach their peak, but its three-dimensional structure underwent reorganization, resulting in a shift in the spatial distribution and intensity of the heat source. The weakened thermal forcing leads to a further southward displacement and reduced intensity of the ascending branch in the anomalous Hadley circulation. Concurrently, the WPSH retreats eastward, and the winds on the western flank of the anomalous anticyclone weakens, resulting in diminished dynamic lifting conditions and moisture transport. Consequently, the middle and lower reaches of the Yangtze River become dominated by subsidence or weak ascending motion, leading to a marked reduction in precipitation and a southward retreat of the rain belt.

This study reveals and establishes a critical physical framework of "three-dimensional oceanic thermal forcing—atmospheric circulation response—regional precipitation" for understanding extreme precipitation events. Diagnostic analysis indicates that the monthly-scale precipitation anomalies in 2020 are closely linked to the monthly evolution of the three-dimensional oceanic thermal structure and its modulation of atmospheric circulation. However, its causal attribution still requires isolating the independent contribution of oceanic thermal forcing from internal atmospheric variability. Previous studies have demonstrated through numerical experiments that sea surface temperature anomalies can modulate atmospheric circulation (Sauvage et al., 2021; Zhang et al., 2023). Based on this framework, future studies could employ numerical sensitivity simulations to

further verify the dominant role of this process chain in different extreme precipitation events, which holds substantial significance for improving climate models.

Funding

This study was supported by the project "Atmospheric Fluid Mechanics" (2020KCSZ01), a Provincial-level Demonstration Course for Curriculum-based Ideological and Political Education of Sichuan Province.

Conflicts of Interest

The authors declare no conflicts of interest regarding the publication of this paper.

References

Bai, Q. M., He, S. F., Feng, A. Q., Li, Z., Chen, C. B., & Yan, J. H. (2025). A Dataset of Heat Wave and Drought Indices in the Middle and Lower Reaches of the Yangtze River from 1961 to 2020. *China Scientific Data, 10,* 46-59. https://doi.org/10.11922/11-6035.csd.2024.0139.zh

Cao, T. W., Zheng, F., & Fang, X. H. (2022). Key Processes on Triggering the Moderate 2020/21 La Niña Event as Depicted by the Clustering Approach. *Frontiers in Earth Science, 10,* Article ID: 822854. https://doi.org/10.3389/feart.2022.822854

Carton, J. A., & Giese, B. S. (2008). A Reanalysis of Ocean Climate Using Simple Ocean Data Assimilation (SODA). *Monthly Weather Review, 136,* 2999-3017. https://doi.org/10.1175/2007mwr1978.1

Chen, C., Xu, C. Y., Qin, J. H., Kang, Y. Y., & Wang, G. F. (2024). The Spatial and Temporal Differences of Upper Ocean in Tropical Pacific during the "Triple-Dip" La Niña of 2020-2023. *Journal of Marine Sciences, 42,* 12-20.

Ding, Y. H., Liu, J. J., & Sun, Y. (2007). A Study of the Synoptic-Climatology of the Meiyu System in East Asia. *Chinese Journal of Atmospheric Sciences, 31,* 1082-1101.

Gong, Z. S., & He, M. (2006). Relationship between Summer Rainfall in Changjiang River Valley and SSTA of Various Seasons. *Meteorological Monthly, 32,* 56-61.

Hersbach, H., Bell, B., Berrisford, P., Hirahara, S., Horányi, A., Muñoz-Sabater, J. et al. (2020). The ERA5 Global Reanalysis. *Quarterly Journal of the Royal Meteorological Society, 146,* 1999-2049. https://doi.org/10.1002/qj.3803

Huang, B., Liu, C., Banzon, V. F., Freeman, E., Graham, G., & Hankins, W. (2020). *NOAA 0.25-Degree Daily Optimum Interpolation Sea Surface Temperature (OISST), Version 2.1 [Data Set]*. NOAA National Centers for Environmental Information.

Huang, R. H., & Sun, F. Y. (1994). Impact of the Convective Activities over the Western Tropical Pacific Warm Pool on the Intraseasonal Variability of the East Asian Summer Monsoon. *Chinese Journal of Atmospheric Sciences, 18,* 456-465.

Huang, R. P., Chen, S. F., Chen, W., Yu, B., Hu, P., Ying, J., & Wu, Q. Y. (2021). Northern Poleward Edge of Regional Hadley Cell over Western Pacific during Boreal Winter: Year-to-Year Variability, Influence Factors and Associated Winter Climate Anomalies. *Climate Dynamics, 56,* 3643-3664. https://doi.org/10.1007/s00382-021-05660-9

Jiang, T., Zhai, J. Q., Luo, Y., Su, B. D., Chao, Q. C., Wang, Y. J. et al. (2022). Progress in Assessment Reports on the Impacts, Adaptation, and Vulnerability of Climate Change: New Insights from IPCC AR5 to AR6. *Transactions of Atmospheric Sciences, 45,* 502-511.

Li, X., Zhang, K., Gu, P. R., Feng, H. T., Yin, Y. F., Chen, W., & Cheng, B. C. (2021). Changes in Precipitation Extremes in the Yangtze River Basin during 1960-2019 and the Association with Global Warming, ENSO, and Local Effects. *Science of the Total Environment, 760,* Article ID: 144244. https://doi.org/10.1016/j.scitotenv.2020.144244

Li, Y., Wang, Y. F., & Wei, D. (2007). Effects of Anomalous SST in Tropical Indian Ocean and Pacific Ocean on Next June Rainfall over the Yangtze River Basin and Area South of the Basin. *Acta Meteorologica Sinica, 65,* 393-405.

Liu, Y. Y., & Ding, Y. H. (2020). Characteristics and Possible Causes for the Extreme Meiyu in 2020. *Meteorological Monthly, 46,* 1393-1404.

Liu, Y. Y., Wang, Y. G., & Ke, Z. J. (2021). Characteristics and Possible Causes for the Climate Anomalies over China in Summer 2020. *Meteorological Monthly, 47,* 117-126.

Ma, J., Wei, K., & Chen, W. (2022). Self-Maintaining Mechanism of a Large-Scale Persistent Heavy Rainfall Event in Mei-Yu Period: Case Study of Yangtze River Heavy Rainfall in 2020. *Chinese Journal of Atmospheric Sciences, 46,* 1394-1406.

Ou, L. J., Yu, J. H., Zhong, X. Y., Zhang, W. X., Liu, Y. J., Wang, Y. et al. (2022). Impacts of the SST Warming Trend and Natural Variability on the Summer Extreme Precipitation Intensity of the Middle and Lower Reaches of the Yangtze River. *Chinese Journal of Atmospheric Sciences, 46,* 1595-1606.

Sauvage, C., Lebeaupin Brossier, C., & Bouin, M. (2021). Towards Kilometer-Scale Ocean-Atmosphere-Wave Coupled Forecast: A Case Study on a Mediterranean Heavy Precipitation Event. *Atmospheric Chemistry and Physics, 21,* 11857-11887. https://doi.org/10.5194/acp-21-11857-2021

Tang, Y. L., Xu, G. R., & Wan, R. (2022). Temporal and Spatial Distribution Characteristics of Short-Duration Heavy Rainfall in the Yangtze River Basin during the Main Flood Season of 2020. *Transactions of Atmospheric Sciences, 45,* 212-224.

Wang, B., Wu, R. G., & Fu, X. H. (2000). Pacific-East Asian Teleconnection: How Does ENSO Affect East Asian Climate? *Journal of Climate, 13,* 1517-1536. https://doi.org/10.1175/1520-0442(2000)013<1517:peathd>2.0.co;2

Wang, Y. G., Lou, D. J., & Liu, Y. Y. (2020). Characteristics and Causes Analysis of Abnormal Meiyu Rainfall in the Middle and Lower Reaches of Yangtze River Valley in 2020. *Torrential Rain and Disasters, 39,* 549-554.

Wu, X. F., Zhang, Q. L., & Liu, Z. H. (2014). Annual and Interannual Variations of the Western Pacific Warm Pool Volume and Sources of Warm Water Revealed by Argo Data. *Science China Earth Sciences, 57,* 2269-2280. https://doi.org/10.1007/s11430-014-4893-5

Zhang, S. J., Li, Z. J., Ma, W. L., Jiang, X. L., Zhou, W., & Fei, J. F. (2023). A Preliminary Study on the Impacts of Air-Sea-Wave Coupling on Short-Term Numerical Weather Prediction in Southeast China. *Chinese Journal of Atmospheric Sciences, 47,* 1129-1146.

Zhao, Q. F., & Zhou, Y. (2024). Prolonged Effects of the Madden-Julian Oscillation on Persistent Rainfall over Eastern China during Summer 2020. *Chinese Journal of Atmospheric Sciences, 48,* 1157-1172.

Zheng, J. Y., & Wang, C. Z. (2021). The Impact of the Three Oceans on the Record-Breaking Heavy Precipitation over the Yangtze River Basin in June 2020. *Science China: Earth Sciences, 51,* 1611-1623.